Advanced Sensor and Energy Materials 1 (2022) 100026

Contents lists available at ScienceDirect

Advanced Sensor and Energy Materials

journal homepage: www.sciencedirect.com/journal/advanced-sensor-and-energy-materials

Full Length Article

Transmembrane transport characterization across ionic redox transistors using surface-tracked scanning ion conductance microscopy

Vijay Venkatesh *, Travis Hery, Vishnu Baba Sundaresan

Department of Mechanical and Aerospace Engineering, The Ohio State University, 201 W 19th Ave, Columbus, OH, 43210, USA

ARTICLE INFO

Key words:
Ionic redox transistor
Shear-force
Transmembrane transport
Scanning ion conductance microscopy

ABSTRACT

A fundamental understanding of ion transport at the nanoscale is critical to the development of efficient chemical separation membranes, catalysts, ionic/bio-inspired materials, and its scale up into multi-functional ionic devices. Electrochemical imaging using scanning probe microscopy hardware has provided a method to visualize and understand processes that occur at the surface of ionic active materials. The suite of scanning probe microscopy techniques developed over the last few years are limited to imaging surface-level phenomena and have not been applied to investigate transmembrane properties of synthetic and natural membranes with high spatial and temporal resolution. In this article, we demonstrate the application our recently developed 'surface-tracked scanning ion conductance microscopy' technique to characterize voltage-regulated ion transport in an ionic redox transistor. The ionic redox transistor exhibits controlled transmembrane ion transport as a function of its electrochemical redox state. The technique presented in this article uses shear force measured between the nanopipette and ionic substrate to image topography of the porous substrate and simultaneously characterize topography-correlated transmembrane transport through the ionic redox transistor. The transmembrane conductance measured across an array of pores within the ionic redox transistor varies from 0.004 μS/cm (OFF state) to 0.015 μS/cm (ON state). We anticipate that the spatial correlation of transmembrane ion transport in the ionic redox transistor would result in a scale up into smart membrane separators for energy storage, neuromorphic circuits, and desalination membranes.

1. Introduction

Characterization of transmembrane ion transport through porous substrates at the nanoscale is critical to integrating membrane separators in drug delivery [1], gating circuits [2], and batteries [3]. The suite of existing scanning probe microscopy techniques are limited to investigating ion transport as a surface phenomena and do not provide an insight into the fundamental mechanisms of ion transport within the material under investigation. In a recent article, we introduced 'surface-tracked scanning ion conductance microscopy' as a high-resolution microscopy technique to quantitatively characterize transmembrane ion transport across porous substrates [4]. The objective of this paper is to extend the aforementioned technique to enhance our understanding of ion transport across an electrochemical arrangement referred to as an 'ionic redox transistor'. An ionic redox transistor is a device that was developed previously [5] to regulate transmembrane transport and mitigate thermal runaway in commercial Li-ion batteries.

Conducting polymers such as polypyrrole (PPy) doped with anions such as dodecylbenzenesulfonate (DBS^-), polystyrenesulfonate (PSS^-) and dodecylsulfate (DS^-) are attractive candidates for regulating ion transport due to insertion/expulsion of cations into/out of the polymer backbone during the reduction/oxidation [6]. The concept of using conducting polymers as an 'ionic gate' was first proposed by Murray and Burgmayer [7,8]. It was noted that the membrane switches between an ON-OFF state during reduction/oxidation of the polymer, thus resulting in controlled ion transport. Price and coworkers extended this principle to develop ion-transport systems for separating various metal ions from aqueous solutions [9]. They showed that the application of a pulsed potential waveform to the conducting polymer results in higher ionic flux. Misoska and coworkers investigated permeability characteristics of polypyrrole doped with bathocuproinedisulfonic acid (BCS^-) to transition metal ions such as Co^{2+}, Ni^{2+}, Zn^{2+} [10]. To achieve pulsatile drug delivery, Santini and coworkers fabricated a porous microchip on which a thin film of Au was sputtered [11]. The application of an electric field resulted in expulsion of chemicals across the porous channels in the device. Abidian and coworkers synthesized poly(3,4-ethylene dioxythiophene) nanotubes for transporting dexamethasone as a function of electrochemical state of the polymer [12]. Jeon and coworkers fabricated

* Corresponding author.
E-mail address: venkatesh.38@osu.edu (V. Venkatesh).

https://doi.org/10.1016/j.asems.2022.100026
Received 17 May 2022; Received in revised form 15 June 2022; Accepted 20 June 2022
Available online 24 June 2022

a nanoporous membrane consisting of polypyrrole deposited on anodized aluminum oxide for transporting isothiocyanate-labeled bovine serum albumin as a function of redox state of the polymer [13]. It should be mentioned that the conducting polymer was deposited such that the equivalent pore size of the membrane increased/decreased when PPy was oxidized/reduced, thus resulting in greater/lower flux of ions through the nanoporous columns in the substrate. Recently, Hery and Sundaresan fabricated an ionic redox transistor which consists of polypyrrole spanning across the pores of a polycarbonate track-etch membrane [5]. The application of an electric potential to the polymer resulted in bi-directional transport of Li^+ ions across the porous membrane due to hopping pathways created in the polymer backbone. The ionic redox transistor was used as a smart membrane separator in a Li^+ battery to regulate ion transport at elevated temperatures and prevent thermal runaway [14].

Despite aforementioned advances in using conducting polymers for various technologies such as gas filtration [15], gating channels [16] and membrane separators [17], ion transport at the nanoscale in conducting polymers is poorly understood. Although there are a plethora of research articles which have quantified transmembrane properties of synthetic membranes [18,19] using ion conductance microscopy, literature on in-situ imaging of transmembrane ion transport across a membrane separator which can regulate ionic current as a function of its electrochemical signature is limited to a report which investigates increase in equivalent pore size of nanoporous channels deposited with PPy using atomic force microscopy (AFM) [13]. While AFM images of the underlying substrate depicted a change in equivalent pore size as a function of redox state of the polymer, no information was revealed on the variations in ionic flux across the polymer membrane. Further, Laslau and coworkers reported the need for advances in ion conductance microscopy, primarily for the purpose of distinguishing variations in ionic flux of conducting polymers from volumetric expansion due to ion ingress [20]. To address the need for an imaging technique that can quantitatively image ion transport across conducting polymers, this article uses surface-tracked scanning ion conductance microscopy using shear-force (SF) imaging as a technique to investigate kinetics of ion transport in ionic redox transistors.

2. Materials and methods

2.1. Chemicals and apparatus

Aqueous solutions were prepared using deionized water (H_2O, resistivity = 18.2 MΩ cm at 298.15 K, MilliporeSigma, Burlington, MA). A solution of 0.1 M sodium chloride (NaCl, ≥99.5%, MilliporeSigma) was degassed under vacuum in a büchner flask and used as the supporting electrolyte for SICM experiments. Sodium hypochlorite (NaOCl, 10%–15% active chlorine, MilliporeSigma) was used without any modification to prepare Ag/AgCl electrodes (*vide infra*).

2.2. Membrane and nanopipette characterization

Highly ordered microporous Si wafers (62 μm thickness) were purchased from Smart Membranes GmBH, Germany and used as a membrane separator. The pore diameter was estimated from scanning electron microscopy (SEM, FEI Helios Nanolab 600 FIB, Nanosystems Laboratory) as 2.5 μm and is shown in Fig. 1a. Nanopipettes were pulled from borosilicate capillaries as described in the *Supplementary Information*. The inner

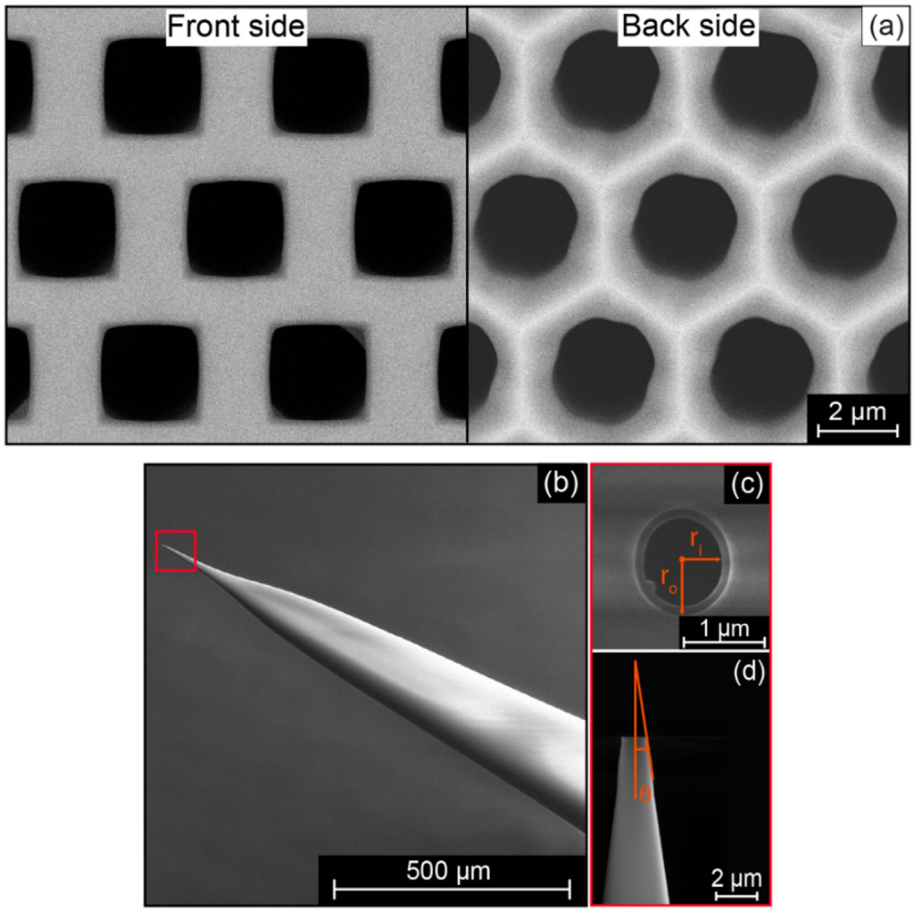

Fig. 1. SEM image of (a) front and back side of the porous Si wafer, (b) anatomy, (c) end-on view, (d) lateral view of the tip.

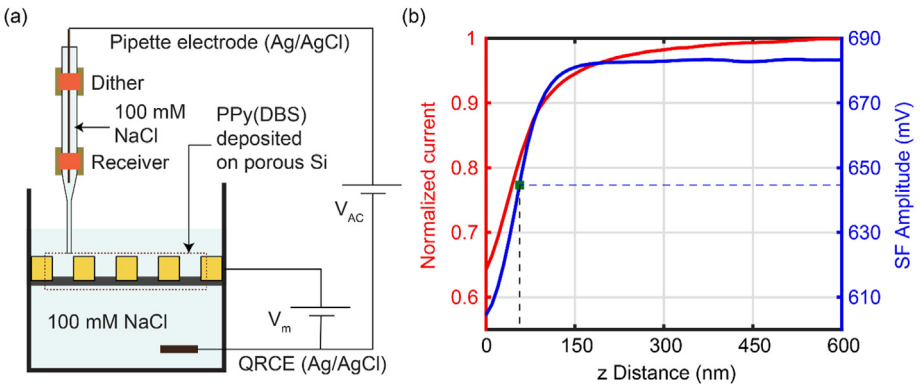

Fig. 2. (a) Schematic representation of the experimental setup, and (b) simultaneously recorded current and SF approach curve over the Si wafer. The set-point voltage at the receiver (645 mV, shown as a symbol on the SF curve) was tracked using a control algorithm to maintain constant SF between the tip and substrate during a raster scan over the substrate for measuring localized transmembrane currents over the Si wafer at various membrane potentials.

radius (r_i) and outer radius (r_o) of the tip were estimated as 0.32 μm and 0.450 μm, respectively, while the half-cone angle (θ) was measured as 10° from the SEM images presented in Fig. 1(b–d).

2.3. Experimental setup

The experimental setup for characterizing transmembrane transport across the ionic redox transistor is shown in Fig. 2a. The Si wafer was sputtered with 40 nm Au and PPy(DBS) was electropolymerized on the Au-sputtered Si substrate as outlined in the *Supplementary Information*. The ionic circuit was set up using the membrane as a septum in a bicameral device containing 0.1 M NaCl in each chamber. PPy(DBS) spans the pores of the Si wafer and forms a barrier for ion transport between the cis and trans chamber of the bicameral device. The Ag/AgCl electrode within the nanopipette (pipette electrode) was biased at a transmembrane potential (V_{AC}) with respect to a Ag/AgCl quasi-reference counter electrode (QRCE) in the bottom chamber. The sputtered Au-layer between the Si wafer and PPy(DBS) allows for application of an independent electric field to PPy(DBS) (V_m) with respect to the QRCE.

2.4. Imaging experiments

An ELP3 EIProScan scanning electrochemical microscope hardware equipped with an SFU 3 SF sensing unit (HEKA Elektronik Dr. Schulze GmbH, Germany) was used to image ion transport across ionic redox transistors at various membrane potentials. The dither and receiver piezoelectric wafers were mounted onto the nanopipette at a parallel orientation as reasoned elsewhere [21,22]. The sensitive frequency for stimulation was determined from SF characteristics of the nanopipette as described in the *Supplementary Information*. A stimulation voltage of 50 mV was applied to the dither at the sensitive frequency. The nanopipette was positioned in solution bulk and the tip current was recorded along with SF at the receiver. A transmembrane characterization experiment was subsequently performed to demonstrate active ion transport across the membrane separator. The PPy(DBS) membrane was stimulated at increasing reduction potentials (V_m = 0 V to −1 V) and the resulting transmembrane current across the membrane (I_{AC}) was recorded as a function of the gate voltage applied to the membrane (V_m). This procedure was repeated at various transmembrane potentials (V_{AC} = 0.1 V–1 V).

The tip was then lowered to approach the Si wafer at a speed of 0.5 μm/s. The z-approach was stopped when the SF measured at the receiver decreased by approximately 50 mV. Simultaneously, the tip current decreased by approximately 20% of the value recorded in solution bulk as shown in Fig. 2b. The sense-length for SF was lower than that for current response which allows for mapping surface topography of the porous Si membrane along with transmembrane currents at the tip during a raster scan over the membrane [23]. The tip was lifted by 3 μm and a reduction potential (V_m) was applied to the polymer. Localized transmembrane currents over an array of pores was recorded using the surface-tracked three-dimensional scan algorithm developed by our group previously [4]. A slope value of 1.1 × 10^3 mV/μm was used as a feedback gain for regulating the tip at the set point value (645 mV, see

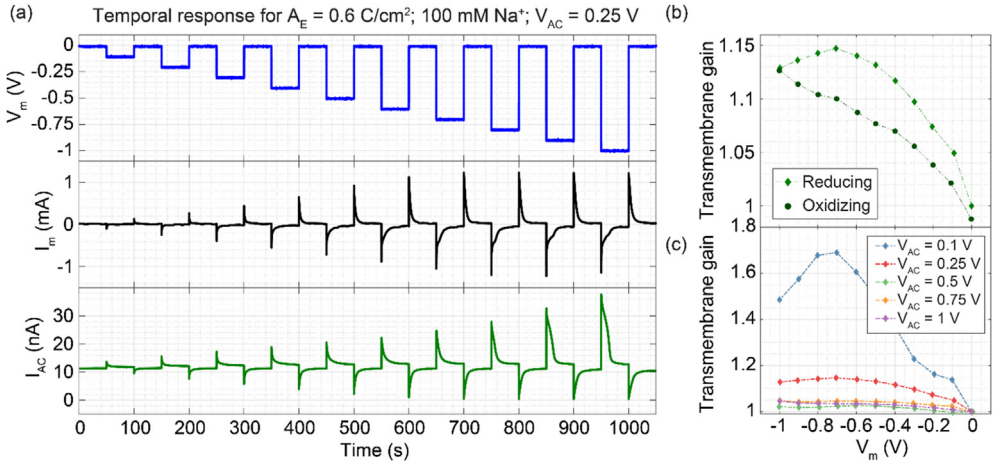

Fig. 3. (a) Typical transmembrane current response (I_{AC}) for a 0.6 C/cm^2 PPy(DBS) polymer in 0.1 M NaCl at different membrane potentials (V_m). The transmembrane potential (V_{AC}) was kept constant at 0.25 V. In the oxidized state (V_m = 0 V), $I_{AC} \approx 0$, and I_{AC} increases with an increase in V_m. (b) Hysteresis in transmembrane gain in reducing and oxidizing directions, and (c) variations in transmembrane gain with V_{AC}.

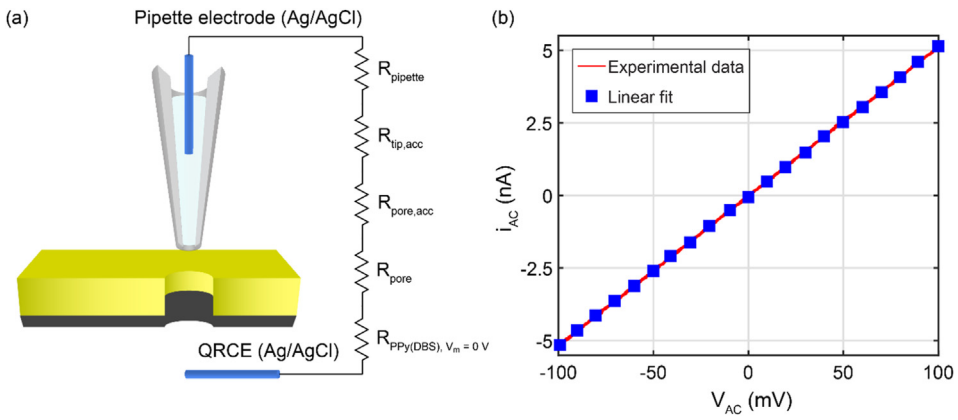

Fig. 4. (a) Equivalent circuit representation of the setup used to characterize ionic redox transistors, and (b) cyclic voltammogram recorded with the tip positioned in solution bulk when the polymer was kept in the oxidized state ($V_m = 0$ V). The total resistance of the system was computed from the voltammogram as 19.42 MΩ.

Table 1
Resistive elements used in the equivalent circuit diagram in Fig. 4a.

Resistive element	Symbol	Formula	Value	Units
Pipette resistance [27]	$R_{pipette}$	$^{1}/_{\pi K r_i \tan(\theta)}$	4.90	MΩ
Access resistance at the tip [28]	$R_{tip,\ acc}$	$\frac{\frac{3}{2}\log\left(\frac{r_o}{r_i}\right)}{\pi K t}$	0.05	MΩ
Access resistance at the end of a pore [29]	$R_{pore,\ acc}$	$\frac{1}{4Ka}$	0.20	MΩ
Pore resistance [30]	R_{pore}	$\frac{L}{\pi K a^2}$	12.76	MΩ
PPy(DBS) resistance in the oxidized state	$R_{PPy(DBS),\ V_m=0}$	$R_{total} - R_{pipette} - R_{tip,acc} - R_{pore,acc} - R_{pore}$	1.51	MΩ
Total resistance	R_{total}	Obtained from voltammogram	19.42	MΩ

Fig. 2a). The tip was raster scanned across a 100 μm^2 area over the Si membrane at a scanning speed of 1.25 μm/s to simultaneously record surface topography and localized transmembrane currents.

3. Results and discussion

3.1. Transmembrane characterization

Fig. 3a depicts the temporal response in transmembrane current (I_{AC}) across the ionic redox transistor as a function of reduction potential (V_m) applied to PPy(DBS). The transmembrane potential across the ionic redox transistor was kept constant at 0.25 V. We note that transmembrane currents are negligible (I_{AC}~0) till the onset of a threshold reduction potential ($V_m < -0.4$ V) and the membrane is in the OFF state. Beyond this reduction potential, the electroneutrality of the polymer changes and a net negative charge gathers on the polymer. Cations from the electrolyte (Na^+) ingress into the DBS^- dopant sites in the polymer to maintain electroneutrality [24]. These dopant ions serve as 'hopping sites' in the polymer bulk and facilitate ion transport across PPy(DBS) [25]. Consequently, the transmembrane current (I_{AC}) begins to increase as the applied membrane potential decreases beyond this threshold reduction potential and the membrane reaches its ON state. When the applied potential to the membrane decreases beyond the peak reduction potential ($V_m < -0.7$ V), the transmembrane current reaches a steady state value due to saturation in the number of hopping sites in the polymer. Due to the functional similarities with a field effect transistor, this arrangement has been referred to as an 'ionic redox transistor' in literature [5].

Fig. 3b shows peak-to-peak transmembrane gain from the temporal response plotted as a function of the applied potential to PPy(DBS). The transmembrane gain (β) is computed by scaling the measured transmembrane current in the reduced state ($I_{AC,\ V_m}$) to the transmembrane

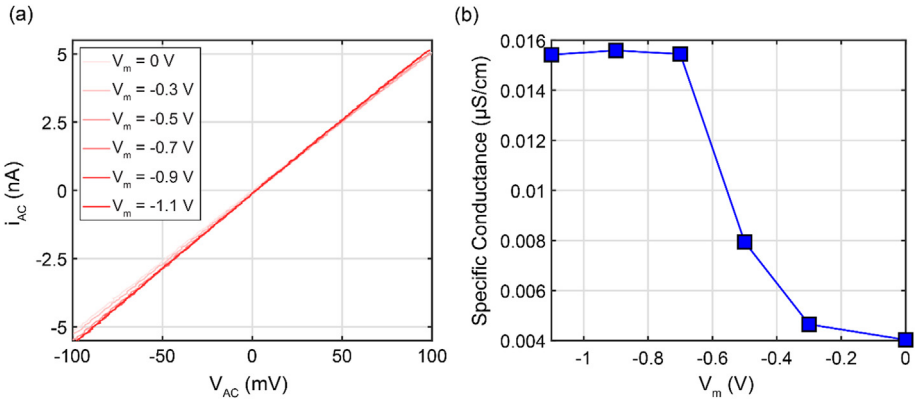

Fig. 5. (a) Cyclic voltammogram recorded at various membrane potentials (V_m), (b) Specific conductance (σ_{V_m}) of PPy(DBS) as a function of the potential applied to the membrane (V_m).

Table 2
Resistance of PPy(DBS) ($R_{PPy(DBS),\ V_m}$) as a function of the potential applied to the polymer (V_m). The transmembrane potential was swept between −100 mV and 100 mV (see Fig. 5).

Potential (V_m) (V)	0	−0.3	−0.5	−0.7	−0.9	−1.1
Resistance of PPy(DBS) (MΩ) ($R_{PPy(DBS),\ V_m}$)	1.517	1.346	0.829	0.435	0.431	0.437

current in the OFF state ($I_{AC,\ V_m=0}$). Thus,

$$\beta = \frac{I_{AC,\ V_m}}{I_{AC,\ V_m=0}} \tag{1}$$

We note that the polymer switches between its fully OFF and fully ON state as the reduction potential (V_m) applied to PPy(DBS) increases from 0 to −0.7 V. This indicates that transmembrane transport through PPy(DBS) can be regulated between a minimum value and a maximum value in real-time. Further, Fig. 3b depicts a hysteresis in transistor characteristics as a function of V_m. This unintended, yet useful outcome demonstrates that the conductance of the ionic redox transistor for an applied potential V_m switches between two discrete memory states depending on whether the polymer was initially oxidized/reduced. This functionality makes the ionic redox transistor as an attractive candidate for interesting applications such as neuromorphic computing and memristive circuitry [26].

The effects of transmembrane potential (V_{AC}) on ionic redox transistor characteristics are plotted in Fig. 3c. While the variations in transistor characteristics are negligible for higher transmembrane potentials ($V_{AC} \geq 0.25$ V), an abnormally high transmembrane gain is obtained when the applied transmembrane potential equals 0.1 V. The reader is advised not to confuse the transmembrane gain computed in this experiment with the 'amplification factor' coined by Hery and Sundaresan [5] due to differences in the equivalent circuit configuration (see Section 3.2).

3.2. Equivalent circuit configuration

The equivalent circuit configuration of the system is shown in Fig. 4a. The total resistance of the system was estimated from cyclic voltammetry. The tip was positioned in solution bulk (~2 μm) above a pore. Fig. 4b presents the cyclic voltammogram recorded between −100 mV and 100 mV (scan rate = 25 mV/s) with the PPy(DBS) in the oxidized state (V_m = 0 V). The total resistance of the system was estimated as 19.42 MΩ and can be described by the circuit elements shown in Fig. 4a. It is to be noted that the PPy(DBS) membrane deposited on the substrate serves as a variable resistor and its resistance is dependent on the reduction potential applied to the membrane. Mathematically, the total resistance of the system can be computed from the pore length in the Si wafer (L = 62 μm), conductivity of 0.1 M NaCl ($K = 9.9 \times 10^{-7}$ S/μm at 298.15 K), pore radius (a = 1.25 μm (see SEM image in Fig. S1(c)), distance of the tip above a pore (t = 2 μm), inner radius (r_i = 0.372 μm), outer radius (r_o = 0.450 μm), and half-cone angle (θ = 10°) of the nanopipette using analytical expressions presented in Table 1.

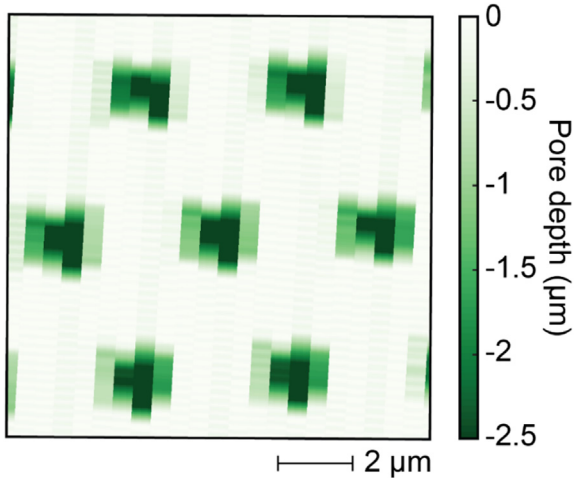

Fig. 6. Topography of the porous Si wafer mapped during SICM-SF. The tip regulates about the set point value (645 mV) during a raster scan over the membrane.

The resistance of the PPy(DBS) membrane is obtained from the analytical expression presented in Table 1 as 1.51 MΩ. The specific conductivity of the polymer in the oxidized state ($\sigma_{V_m=0}$) can be calculated as

$$\sigma_{V_m=0} = \frac{t_o}{A_{pore} R_{PPy(DBS),\ V_m=0}} \tag{2}$$

where t_o is the thickness of PPy(DBS) in the oxidized state (3 μm, see Fig. S2) and A_{pore} is the pore area. The conductance of the polymer in the oxidized state computed from Equation (2) was 0.004 μS/cm.

3.3. Transistor characteristics

Transmembrane characteristics of the ionic redox transistor was estimated from the cyclic voltammogram shown in Fig. 5a. The voltammogram depicts variations in total resistance of the system (R_{total}) as a function of the redox potential applied to the polymer (V_m). Although the total resistance of the system (R_{total}) changes by approximately 1 MΩ, the change in resistance is barely noticeable due to the dominant effect of pore/pipette resistance. The resistance of PPy(DBS) ($R_{PPy(DBS),\ V_m}$) as a function of the potential applied to the polymer (V_m) is computed using the approach presented in the previous Section and is shown in Table 2. The conductance of the polymer as a function of its redox state (σ_{V_m}) can be computed as

$$\sigma_{V_m} = \frac{t_o(1+\epsilon)}{A_{pore} R_{PPy(DBS),\ V_m=0}} \tag{3}$$

where ϵ is the strain produced in PPy(DBS) due to cation ingress. The strain produced in the polymer was obtained from mechanoelectrochemistry experiments presented in the *Supplementary Information*. Fig. 5b shows the conductivity of PPy(DBS) as a function of its redox state. Note that ionic conductance of PPy(DBS) increases as the reduction potential applied to the membrane (V_m) increases, fittingly exhibiting a transistor-like behavior. The change in ionic conductivity between oxidized and reduced states as measured from this experiment is consistent with the trend reported in literature [5].

3.4. Analysis of localized currents using SICM-SF

3.4.1. Topography characterization

SICM-SF was used to map localized transmembrane currents over an array of pores at different membrane potentials (V_m). Fig. 6 shows topography of the Si wafer mapped during a 100 μm^2 scan area above the membrane. The tip exhibits a reproducible descent-ascent into and out of each pore while regulating about the set point value (645 mV, see Fig. 2a). The total time taken to scan the surface at a speed of 1.25 μm/s (31 line scans) was estimated using Equation (4) and was approximately 5 min.

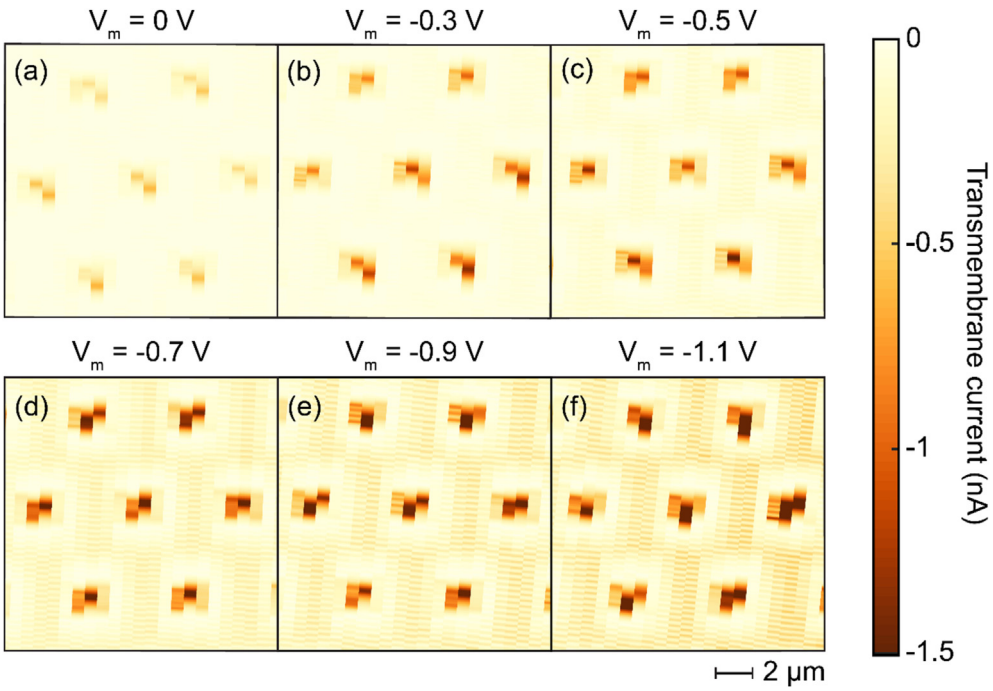

Fig. 7. Localized transmembrane currents measured over each pore at various membrane potentials (V_m). The transmembrane potential (V_{AC}) was kept constant at 0.1 V.

$$t_e = \frac{nX}{s_x} \tag{4}$$

3.4.2. Interpretation of localized transmembrane currents

Localized transmembrane currents over each pore was recorded at various membrane potentials (V_m) using surface-tracked SICM and is shown in Fig. 7. The transmembrane potential in this experiment was kept constant at 0.1 V. As the tip moves into and out of each pore, note that local transmembrane currents over a pore increase with an increase in V_m. This increase in local transmembrane currents is of the order of 1 nA and can be attributed to an overall increase in resistance between the pipette electrode (PE) and QRCE. According to the Goldman-Hodgkin-Katz (GHK) Equation described in our earlier work [4], the ionic current ($i^{\pm}(x)$) measured at the nanopipette over a pore can be described by

$$i^{\pm}(x) = F\left(\frac{2a_p^2 D^{\pm} z^{\pm} \Delta}{L}\right) \tan^{-1}\left(\frac{a_p\sqrt{2}}{\sqrt{\left(x^2+2d^2-a_p^2\right)+\sqrt{\left(x^2+2d^2-a_p^2\right)^2+4d^2a_p^2}}}\right) \left(\frac{C_l^{\pm} - C_u^{\pm} e^{-z^{\pm}\Delta}}{1-e^{-z^{\pm}\Delta}}\right) \tag{5}$$

where F is the Faraday constant, a_p is the pore radius from the line scan, $D^{\pm}$ is the diffusion coefficient of the cation/anion, $z^{\pm}$ is the charge on cation/anion, Δ is the potential drop between the PE and QRCE, L is the length of the pore, x is the horizontal distance of the tip from the center of a pore, d is the height of the tip above a pore, $C_l^{\pm}$ is the electrolyte concentration in the trans (lower) chamber, and $C_u^{\pm}$ is the electrolyte concentration in the cis (upper) chamber. The local transmembrane currents measured at the tip (I_{AC}) is computed from Equation (5) as

$$I_{AC}(x) = \varepsilon\left(z^{+}i^{+}(x) + z^{-}i^{-}(x)\right) \tag{6}$$

As the PPy(DBS) polymer is stimulated at increasing reduction potentials (V_m), the total resistance of the polymer decreases (see Table 2). This decrease in total resistance of the system increases the potential difference between the QRCE and PE according to the relation $\varphi = -R_{pore}V_{PE}/R_{sys}$, which consequently results in an increase in Δ. This increase in Δ increases the absolute magnitude of local transmembrane currents over each pore according to Equation (5) and Equation (6).

4. Conclusions

In this article, surface-tracked scanning ion conductance microscopy is used to investigate bi-directional ion transport across an ionic redox transistor. It was shown that an application of a reduction potential to PPy(DBS) (V_m) under a constant transmembrane potential (V_{AC}) facilitates ion ingress into redox sites in the polymer and drives transmembrane transport. The transmembrane current increases as the potential applied to PPy(DBS) (V_m) increases, thus switching the transistor from its OFF state to its ON state. An equivalent circuit model of the system was developed and it was shown that the transmembrane current was a result of an increase in conductivity of the polymer under a reduction potential. Finally, surface-tracked scanning ion conductance microscopy was used to map topography and topography-correlated transmembrane transport over an array of pores. The increase in local transmembrane currents was attributed to a higher potential drop between the PE and QRCE, and was quantified using a modified Goldman-Hodgkin-Katz (GHK) Equation. It is anticipated that surface-tracked scanning ion conductance microscopy would serve as a tool to characterize transmembrane ion transport across various ionic devices used in chemical separation, gas filtration drug delivery, and desalination.

Conflicts of interest

The authors declare no competing conflict of interest.

Acknowledgments

Financial support was provided by the member organizations of the Smart Vehicle Concepts Center, a Phase III National Science Foundation Industry-University Cooperative Research Center (www.SmartVehicleCenter.org) under grant NSF IIP 1738723.

Appendix A. Supplementary data

Supplementary data to this article can be found online at https://doi.org/10.1016/j.asems.2022.100026.

References

[1] D. Svirskis, J. Travas-Sejdic, A. Rodgers, S. Garg, Electrochemically controlled drug delivery based on intrinsically conducting polymers, J Contr Release 146 (1) (2010) 6–15.

[2] D.A. Bernards, G.G. Malliaras, G.E. Toombes, S.M. Gruner, Gating of an organic transistor through a bilayer lipid membrane with ion channels, Appl Phys Lett 89 (5) (2006), 053505.

[3] P. Gilmore, V.B. Sundaresan, A functionally graded cathode architecture for extending the cycle-life of potassium-oxygen batteries, Batter Supercaps 2 (8) (2019) 662, 662.

[4] V. Venkatesh, C. Heinemann, V.B. Sundaresan, Surface-tracked scanning ion conductance microscopy: a novel imaging technique for measuring topography-correlated transmembrane ion transport through porous substrates, Micron 120 (2019) 57–65.

[5] T. Hery, V.-B. Sundaresan, Ionic redox transistor from pore-spanning PPy (DBS) membranes, Energy Environ Sci 9 (8) (2016) 2555–2562.

[6] V. Venkatesh, N. Katsube, V.B. Sundaresan, Morphology-dependent mass transport model for mechanoelectrochemistry of polypyrrole, Smart Mater Struct 28 (1) (2018), 015001.

[7] P. Burgmayer, R.W. Murray, An ion gate membrane: electrochemical control of ion permeability through a membrane with an embedded electrode, J Am Chem Soc 104 (22) (1982) 6139–6140.

[8] P. Burgmayer, R.W. Murray, Ion gate electrodes. Polypyrrole as a switchable ion conductor membrane, J Phys Chem 88 (12) (1984) 2515–2521.

[9] W. Price, C. Too, G.G. Wallace, D. Zhou, Development of membrane systems based on conducting polymers, Synth Met 102 (1–3) (1999) 1338–1341.

[10] V. Misoska, J. Ding, J. Davey, W. Price, S. Ralph, G.G. Wallace, Polypyrrole membranes containing chelating ligands: synthesis, characterisation and transport studies, Polymer 42 (21) (2001) 8571–8579.

[11] J. Santini, T. John, A.C. Richards, R. Scheidt, M.J. Cima, R. Langer, Microchips as controlled drug-delivery devices, Angew Chem Int Ed 39 (14) (2000) 2396–2407.

[12] M.R. Abidian, D.H. Kim, D.C. Martin, Conducting-polymer nanotubes for controlled drug release, Adv Mater 18 (4) (2006) 405–409.

[13] G. Jeon, S.Y. Yang, J. Byun, J.K. Kim, Electrically actuatable smart nanoporous membrane for pulsatile drug release, Nano Lett 11 (3) (2011) 1284–1288.

[14] T. Hery, V.B. Sundaresan, Controlled operation of lithium ion batteries using reversible shutdown membrane separators, smart materials, adaptive structures and intelligent systems, Am Soc Mech Eng (2019), V001T07A004.

[15] M.R. Anderson, B.R. Mattes, H. Reiss, R.B. Kaner, Gas separation membranes: a novel application for conducting polymers, Synth Met 41 (3) (1991) 1151–1154.

[16] J. Zhang, M. Li, E.T. Kang, K.G. Neoh, Electrical stimulation of adipose-derived mesenchymal stem cells in conductive scaffolds and the roles of voltage-gated ion channels, Acta Biomater 32 (2016) 46–56.

[17] A. Kausar, Overview on conducting polymer in energy storage and energy conversion system, J Macromol Sci Phys, Part A 54 (9) (2017) 640–653.

[18] L. Yao, F.P. Filice, Q. Yang, Z. Ding, B. Su, Quantitative assessment of molecular transport through sub-3 nm silica nanochannels by scanning electrochemical microscopy, Anal Chem 91 (2) (2018) 1548–1556.

[19] C.L. Bentley, M. Kang, S. Bukola, S.E. Creager, P.R. Unwin, High-resolution ion-flux imaging of proton transport through Graphene| nafion membranes, ACS Nano 16 (4) (2022) 5233–5245.

[20] C. Laslau, D.E. Williams, B.E. Wright, J. Travas-Sejdic, Measuring the ionic flux of an electrochemically actuated conducting polymer using modified scanning ion conductance microscopy, J Am Chem Soc 133 (15) (2011) 5748–5751.

[21] V. Venkatesh, R. Northcutt, C. Heinemann, V.B. Sundaresan, A structural model of ultra-microelectrodes for shear-force based scanning electrochemical microscopy, J Intell Mater Syst Struct 29 (18) (2018) 3562–3571.

[22] V. Venugopal, V. Venkatesh, R.G. Northcutt, J. Maddox, V.B. Sundaresan, Nanoscale polypyrrole sensors for near-field electrochemical measurements, Sens Actuators B Chem 242 (2017) 1193–1200.

[23] R.G. Northcutt, C. Heinemann, V.B. Sundaresan, Dynamic mechanoelectrochemistry of polypyrrole membranes via shear-force tracking, Phys Chem Chem Phys 18 (26) (2016) 17366–17372.

[24] V. Venugopal, H. Zhang, R. Northcutt, V.B. Sundaresan, A thermodynamic chemomechanical constitutive model for conducting polymers, Sensor Actuator B Chem 201 (2014) 293–299.

[25] V. Venugopal, T. Hery, V. Venkatesh, V.B. Sundaresan, Mass and charge density effects on the saturation kinetics of polypyrrole doped with dodecylbenzene sulfonate, J Intell Mater Syst Struct 28 (6) (2017) 760–771.

[26] Y. van de Burgt, E. Lubberman, E.J. Fuller, S.T. Keene, G.C. Faria, S. Agarwal, M.J. Marinella, A.A. Talin, A. Salleo, A non-volatile organic electrochemical device as a low-voltage artificial synapse for neuromorphic computing, Nat Mater 16 (4) (2017) 414–418.

[27] M. Lavallée, M. Lavallée, O.F. Schanne, N.C. Hébert, Glass Microelectrodes, Wiley, New York, 1969, 1969.

[28] C.-C. Chen, L.A. Baker, Effects of pipette modulation and imaging distances on ion currents measured with scanning ion conductance microscopy (SICM), Analyst 136 (1) (2011) 90–97.

[29] J.E. Hall, Access resistance of a small circular pore, J Gen Physiol 66 (4) (1975) 531–532.

[30] Y. Zhou, C.-C. Chen, A.E. Weber, L. Zhou, L.A. Baker, Potentiometric-scanning ion conductance microscopy, Langmuir 30 (19) (2014) 5669–5675.